Automated nanomanipulation for nanodevice construction

2012 Nanotechnology 23 065304

(http://iopscience.iop.org/0957-4484/23/6/065304)

Nanotechnology **23** (2012) 065304 (9pp) doi:10.1088/0957-4484/23/6/065304

Automated nanomanipulation for nanodevice construction

Yan Liang Zhang[1,3], Jason Li[1,3], Steve To[2], Yong Zhang[2], Xutao Ye[1], Lidan You[1] and Yu Sun[1,2]

[1] Department of Mechanical and Industrial Engineering, University of Toronto, 5 King's College Road, Toronto, ON, M5S 3G8, Canada
[2] Department of Electrical and Computer Engineering, University of Toronto, 5 King's College Road, Toronto, ON, M5S 3G8, Canada

E-mail: sun@mie.utoronto.ca

Received 24 September 2011, in final form 8 December 2011
Published 17 January 2012
Online at stacks.iop.org/Nano/23/065304

Abstract
Nanowire field-effect transistors (nano-FETs) are nanodevices capable of highly sensitive, label-free sensing of molecules. However, significant variations in sensitivity across devices can result from poor control over device parameters, such as nanowire diameter and the number of electrode-bridging nanowires. This paper presents a fabrication approach that uses wafer-scale nanowire contact printing for throughput and uses automated nanomanipulation for precision control of nanowire number and diameter. The process requires only one photolithography mask. Using nanowire contact printing and post-processing (i.e. nanomanipulation inside a scanning electron microscope), we are able to produce devices all with a single-nanowire and similar diameters at a speed of ∼1 min/device with a success rate of 95% ($n = 500$). This technology represents a seamless integration of wafer-scale microfabrication and automated nanorobotic manipulation for producing nano-FET sensors with consistent response across devices.

(Some figures may appear in colour only in the online journal)

1. Introduction

Nanowire field-effect transistors (nano-FETs) have emerged as ultrasensitive, miniaturized, label-free sensors for detecting low concentrations of chemical and biological molecules for medical and environmental applications (e.g. proteins [1], nucleic acids [2, 3], viruses [4], NO_2 [5], and humidity [6]). Top-down micro- and nano-fabrication is often used for silicon-nanowire sensor construction, such as electron-beam nanolithography followed by dry etching [1], silicon wire thinning via repeated surface oxidation and HF etching processes [7, 8] and anisotropic timed etching of silicon structures [9]. These top-down techniques involve high-processing costs/complexity and low yields associated with e-beam lithography and focused ion beam (FIB), and significant variability across etched devices due to etching non-uniformity across the wafer and high sensitivity to processing conditions.

Alternatively, pre-synthesized nanotubes or nanowires (e.g. silicon nanowires) are of low cost and can be integrated into microstructures to form nano-FET sensors. We recently quantitatively reported that the number, diameter, and doping density of nanowires incorporated into nano-FET devices strongly determine device sensitivity [10]. Existing wafer-scale nanotube/nanowire integration methods, such as directed assembly [11], contact printing [12], and dielectrophoresis [13] enables inexpensive construction of nano-FET devices; however, they are not capable of precisely controlling these parameters (figure 1) and result in significant variations in sensitivity across devices.

By contrast, mechanical nanomanipulation, despite being serial in nature and slower compared with the above-mentioned wafer-scale nanowire integration methods, promises specificity, precision, and programmed motion. A combined use of wafer-scale processes and automated

[3] Shared first co-authorship. Contributed equally.

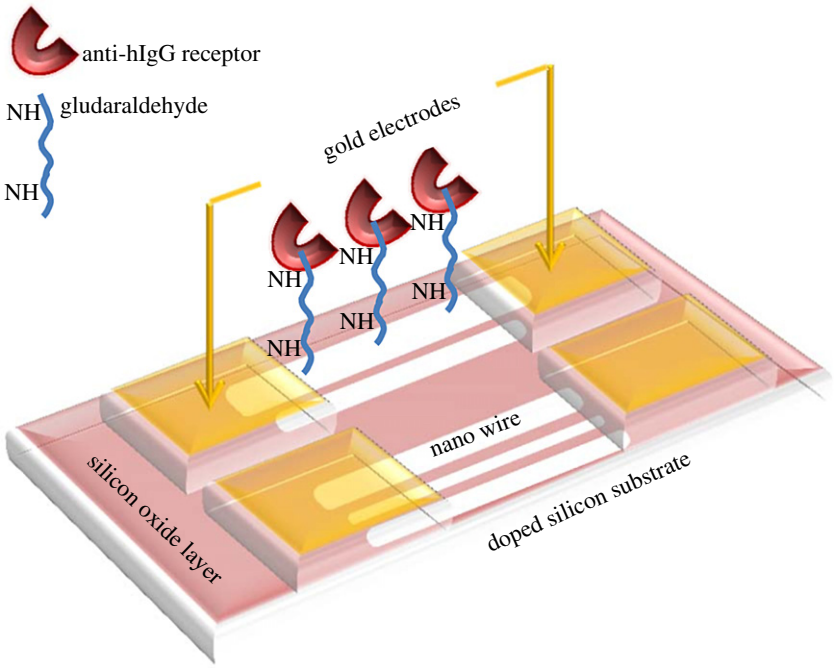

Figure 1. Schematic of nano-FET sensors for sensing hIgG protein. Nanowire diameter and number vary across devices, resulting in sensitivity variations.

nanomanipulation would constitute a new paradigm to bring nanomanufacturing one step further toward scaled-up operation and in the meanwhile, achieve high precision control of nanowire parameters.

Nanomanipulation inside SEM has been largely performed manually by an operator [14–22]. Manual operation requires the operator to carefully monitor the SEM screen and operate joysticks to control the positioning of nanomanipulators. It is time consuming, skill dependent, and has low productivity. Automated nanomanipulation, which uses SEM images as feedback for visually servoing piezoelectric nanomanipulators, demonstrated faster and more repeatable positioning (e.g. [23, 24]).

We previously reported in [10] the effects of nanowire number and diameter on biosensing sensitivity in nano-FET devices. This paper presents details of the nano-FET manufacturing technique. The technique consists of a combined use of wafer-scale fabrication and post-processing via automated nanomanipulation for the construction of nano-FET devices. Silicon nanowires were batch transferred on a substrate, and automated nanomanipulation performed post-processing for precisely controlling the nanowire number and diameter. SEM-vision-based position control enabled the post-processing of nano-FET devices at a speed of $\sim$1 min/device with a success rate of 95% ($n = 500$).

2. System and device batch microfabrication

2.1. Nanomanipulation system

The design of the nanomanipulation system (figure 1(a)) was reported elsewhere [25]. It contains two independent 3-DOF nanomanipulators, both assembled from three linear coarse–fine nanopositioners equipped with optical encoders (resolution: 2 nm). The nanopositioners are capable of operating in either the stick-slip (coarse) mode to produce a large motion range (10 mm) with a step size $\sim$100 nm, or in the fine mode with a 1 μm travel range and a resolution of 1 nm.

The system is small in size ($100 \times 80 \times 46$ mm^3) and capable of being mounted onto and demounted from a standard SEM (e.g. Hitachi SU6600) through the specimen exchange chamber (figure 1(b)) without breaking the high vacuum inside the SEM. The nanomanipulators can be operated manually via joysticks or via computer control.

Tungsten nanoprobes (tip diameter: 200 nm) were chemically cleaned to remove the native tungsten oxide using KOH solutions and HF before they were mounted onto the nanomanipulators. Electrical connections from the nanomanipulators to the outside of the SEM were established through a feedthrough port on the SEM.

2.2. Device batch microfabrication

Phosphorus-doped (n-type) silicon nanowires (10^{17}–10^{19} atoms cm^{-3}, 40–130 nm in diameter) were CVD synthesized. As-grown nanowires were deposited and aligned along a single direction onto a silicon substrate with a 200 nm-thick oxide layer via nanowire contact printing [12]. Nanowires were transferred by scratching the growth substrate against the receiving substrate. The number of nanowires transferred depends on the pressing force between the growth and receiving substrates, the nanowire density on the growth substrate, and the surface properties of the receiving substrate.

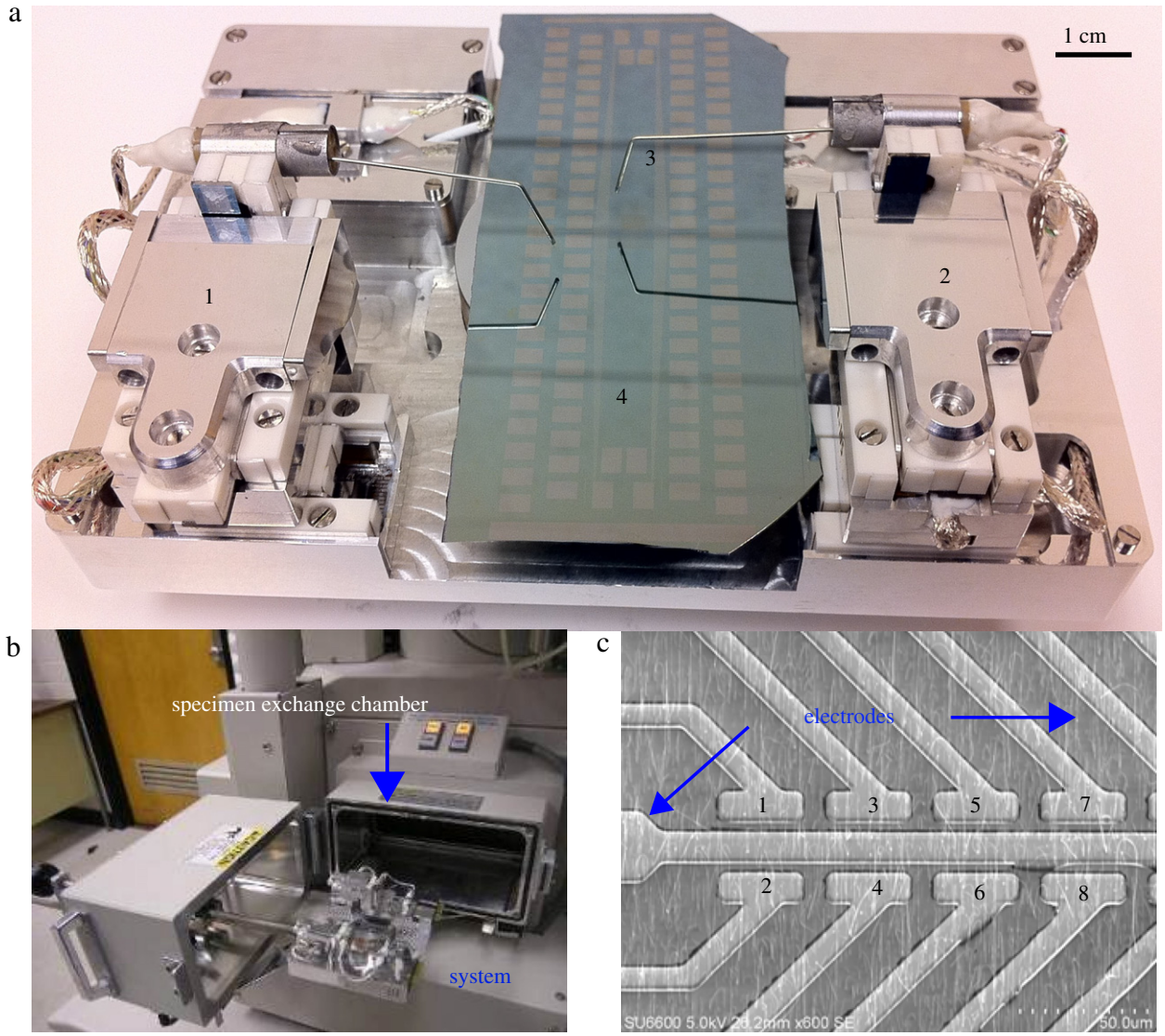

Figure 2. (a) Nanomanipulation system: (1) nanomanipulator-1, (2) nanomanipulator-2, (3) nanoprobe, (4) patterned electrodes pinning nanowires. (b) The system is mounted onto and demounted from the SEM through the specimen exchange chamber. (c) Eight electrode pairs with bridging nanowires underneath.

E-beam evaporation and liftoff were used to form Al microelectrode pairs on top of the nanowires. Figure 1(c) shows eight electrode pairs with bridging nanowires. The gap between the source–drain electrodes was 5 μm on all devices. The figure also shows that different numbers of nanowires bridged each electrode pair since the wafer-scale nanowire contact printing technique is not able to precisely control the number of bridging nanowires, which requires nanomanipulation to post-process the nano-FET devices.

3. Manual nanomanipulation

3.1. Procedures

Manual nanomanipulation for post-processing the wafer-scale fabricated nano-FET devices consists of four major steps as depicted in figure 3. An array of nanowire FET devices (sensors) is first mounted onto the nanomanipulation system and loaded into the SEM. Each device consists of an electrode pair with numerous bridging nanowires that are pinned firmly in place underneath the electrodes (see figure 2(c)). After examination of the nanowire diameters present on each device, the operator selects a suitable nanowire to keep (‘target nanowire’). Preference is given to those nanowires that are located farthest from its neighbors to minimize the likelihood of contact with other nanowires or nanoprobes during the nanowire removal process. The nanowires to be removed are termed ‘unwanted nanowires’.

Before physical removal of unwanted nanowires using the nanoprobes mounted on the nanomanipulators, the operator lowers the nanoprobes until the operator judges that the nanoprobes have established contact with the device substrate. As illustrated in figure 3(c), the operator then uses the joystick to position the nanoprobe tip along the two inner edges of the electrodes for severing unwanted nanowires. Since the nanowires are firmly pinned underneath

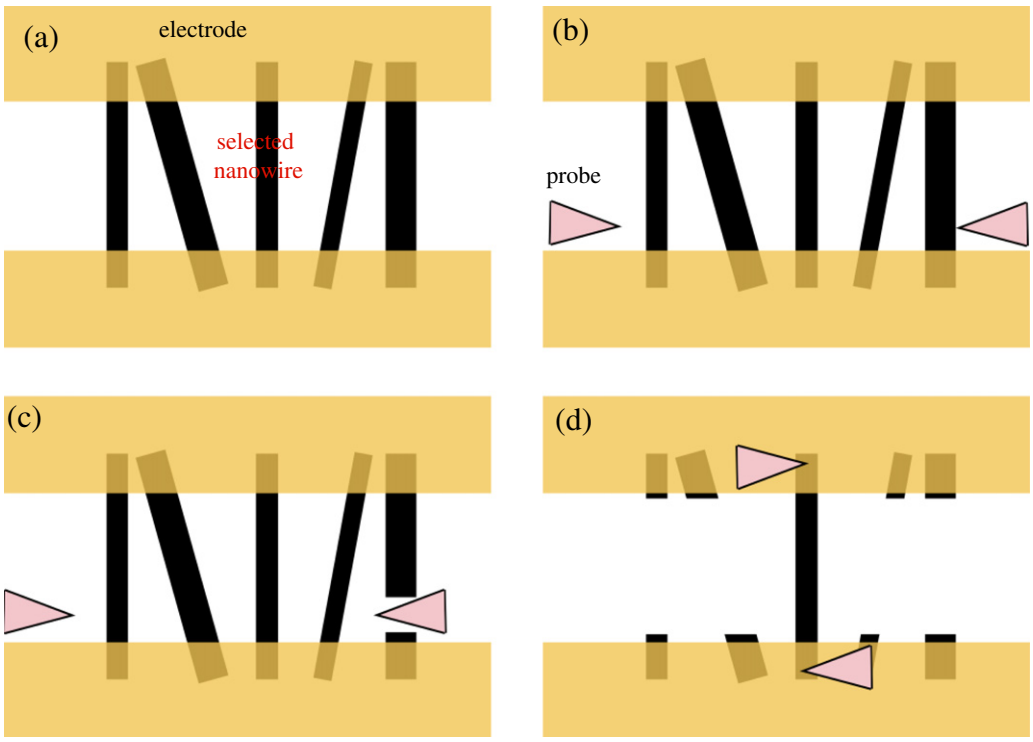

Figure 3. Physical removal of unwanted nanowires. (a) The operator decides which nanowire(s) to keep. (b) The nanoprobes are lowered to the substrate surface. (c) Unwanted nanowires are severed. (d) Electrical property characterization is performed.

the electrodes, nanowire fracture during selective removal is assured to occur along the electrode edges.

Physical interactions with the nanoprobe causes nanowire bending prior to fracture. A bent nanowire may come into contact with adjacent nanowires and, in some cases, cause physical damage to the target nanowire. A severed nanowire may land on top of the target nanowire, forming an undesired nanowire network. Significant care must be taken by the operator in severing nanowires in close proximity to (1) reduce inadvertent damage to the target nanowire due to imprecise nanoprobe movements associated with manual operation control, and (2) reduce the possibility of nanowire networking.

Subsequent to nanowire removal (figure 3(d)), the operator can conduct *in situ* electrical characterization of the target nanowire by placing the two nanoprobes onto the source and drain electrodes, for confirming ohmic contact and measuring the target nanowire's *I*–*V* properties. Devices with significant contact resistance are deemed inappropriate for sensing use and are thus discarded.

3.2. Success rate and efficiency

Success rates and the average time spent processing each device are operator dependent in manual nanomanipulation. Table 1 summarizes the success rate and average processing time for three operators. The three operators all had experience in conducting manual nanomanipulation, and each processed 20 devices to form single-nanowire devices. The data table also details the frequency of occurrence for the two failure cases (i.e. nanowire broken and networked nanowires).

Table 1. Manual nanomanipulation for post-processing 60 devices.

		Unsuccessful		
Operator	Successful	Broken	Networked	Average processing time (min)
1	8	10	2	9
2	12	7	1	12
3	9	10	1	10

The three trained operators produced success rates ranging from ∼40% to ∼60%. The predominant failure case is attributed to accidental nanowire breakage, which resulted from imprecise position control of the nanoprobes. Manual nanomanipulation is also time consuming. On average, it took 10.3 min for an operator to process one nanowire FET device. The total time cost of 10.3 min is from ∼4.5 min for nanowire selection, ∼3.2 min for contact detection, and ∼2.6 min for nanowire removal.

4. Automated nanowire removal

To improve nanomanipulation success rate and efficiency, visual recognition of nanowires and SEM-vision-based position control were developed to automate nanowire FET device post-processing, including nanowire detection and selection, contact detection, and nanowire severing.

4.1. Nanowire detection and selection

As illustrated in figure 4(a), a multi-nanowire device has n bridging nanowires. The parameters associated with each nanowire NW_i include the nanowire diameter (d_i), and the

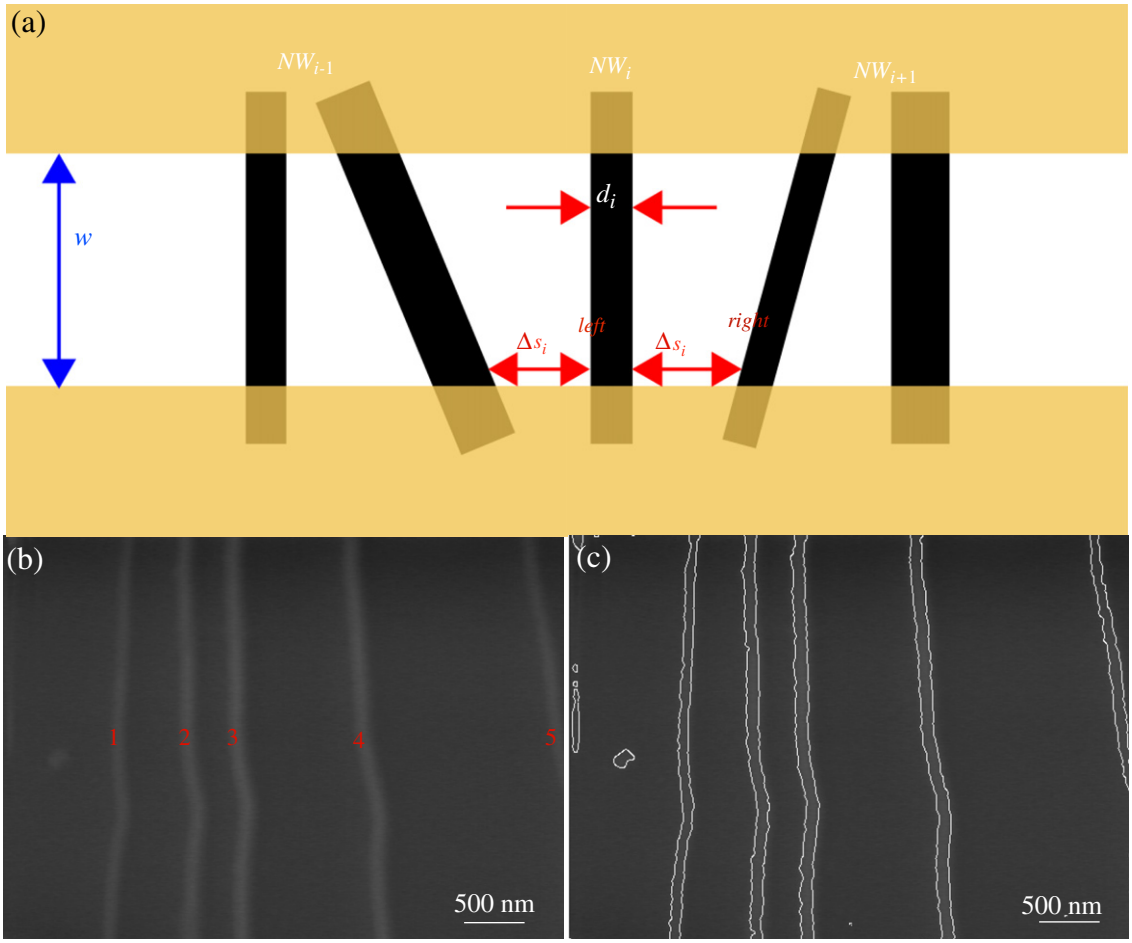

Figure 4. (a) Diameter and distances to adjacent nanowires are determined for each nanowire. (b) A device image showing nanowires bridging electrodes (electrodes not shown in the image). (c) Nanowire contours are extracted from image processing.

distance to the adjacent nanowires (Δs^i_{left} and $\Delta s^i_{\text{right}}$ for the adjacent distances to the left and right, respectively). A nanowire whose Δs^i_{left} and $\Delta s^i_{\text{right}}$ values are larger than a minimum threshold $\Delta S_{\min}$ can be considered a suitable target nanowire candidate. $\Delta S_{\min}$ is the minimum separation distance between two nanowires, which is determined experimentally. Defining $\Delta S_{\min}$ is important such that removal of one nanowire would not damage the other. Among all target nanowire candidates satisfying the $\Delta S_{\min}$ requirement, the nanowire whose diameter is the closest to the desired diameter (d_r) is selected by the system as the target nanowire (i.e. the nanowire to keep). In summary, automated nanowire selection is carried out according to

$$\begin{aligned} \min: \quad & \| d_i - d_r \| \\ \text{subject to}: \quad & \Delta s^i_{\text{left}} \geq \Delta S_{\min} \\ & \Delta s^i_{\text{right}} \geq \Delta S_{\min} \\ & i = 1, \ldots, n. \end{aligned} \tag{1}$$

The system obtains contours of nanowires (see figures 4(b) and (c)) using the greedy snake algorithm [26]. Nanowire diameter d_i is obtained by finding the average width of the contour of nanowire NW_i. Separation distance Δs^i_{left} between nanowire NW_i and NW_{i-1} is determined by locating the shortest distance between points on the left edge of the contour of nanowire NW_i and points on the right edge of the contour of nanowire NW_{i-1} along the electrode edge direction. The system applies the same approach to determine $\Delta s^i_{\text{right}}$. Coordinates of the two end points on the contour of each undesired nanowire near the two electrode edges are also extracted for subsequent position control and nanowire removal.

4.2. Contact detection

We previously summarized our automated contact detection approach in [24]. Briefly, the nanomanipulation system moves a nanoprobe downwards at a constant speed. The position of the nanoprobe tip in the image frame, along its moving direction, is automatically tracked from the SEM images. After nanoprobe–substrate contact is established, further downward motion of the nanoprobe induces a sharp change of probe movement in the image coordinate because of the sliding motion of the nanoprobe on the substrate. The system detects this image coordinate change for determining contact between the nanoprobe and the substrate surface. As shown in figure 5, the nanoprobe contacts the substrate at point A. When the nanoprobe slides slightly on the substrate,

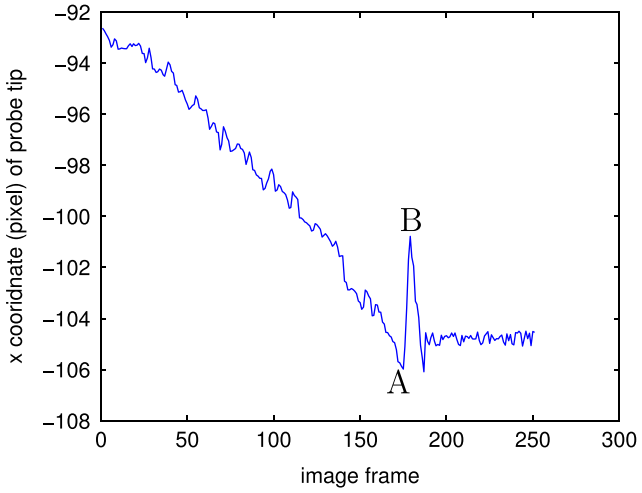

Figure 5. Contact detection. The nanoprobe contacts the substrate at point A. The system detects contact at point B.

for example, by six pixels in the x coordinate, the system determines that contact is established. In experiments, contact detection location on the device substrate was chosen to be $\sim$3 μm away from the target nanowire.

4.3. Nanowire removal

The system uses look-then-move for the XY position control of the nanomanipulators. The system obtains the coordinate difference between the probe and the target position in the image frame as $(\Delta x, \Delta y)$ using image processing. Through coordinate transform, $(\Delta x, \Delta y)$ is converted to (X_d, Y_d) in the world frame of the nanomanipulator. For the X-axis control, X_d is the reference input to the closed-loop control system, as shown in figure 6, which also applies to the Y direction. Encoders integrated in the nanomanipulators provide position feedback X_c along the X direction. Due to the limited travel range of the piezoactuator, the piezomotor (coarse) is used to bring the probe to within the fine travel range of the target position. The piezoactuator (fine) then is switched on to bring the probe precisely to the target position. Hence, voltage input to the nanomanipulators is

$$\begin{aligned} U_c, E &\geq \text{travel range of piezoactuator} \\ U_f, E &< \text{travel range of piezoactuator} \end{aligned} \tag{2}$$

where U_c and U_f are both generated by the PID control law. In experiments, the sampling frequency of the encoders was set to 100 Hz. The control gains were tuned through trial and error. For a travel distance of 250 μm, it takes 0.25 s for the system to reach the steady state.

5. Results and discussion

5.1. Nanowire selection

The desired nanowire diameter d_r can be user specified for a group of nano-FET devices such that sensitivity variations

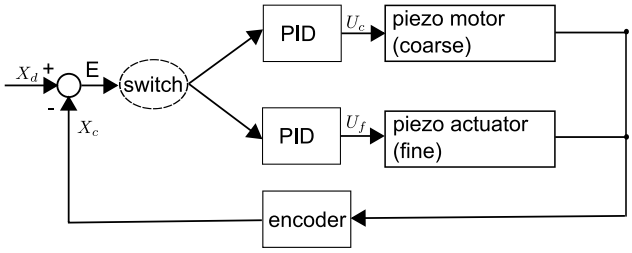

Figure 6. Look-then-move and closed-loop position control.

Table 2. Effect of $\Delta s_{\min}$ value on the number of qualified NWs within each device.

$\Delta s_{\min}$ (μm)	5	3	2	1	0.5
Average number of NW candidates	1.2	2.5	4	7	12

Table 3. Effect of $\Delta s_{\min}$ value on failure rate of NW severing.

$\Delta s_{\min}$ (μm)	5	3	2	1	0.5
Fail (%)	0	0	1	4	12

across these devices are suppressed. The rational selection of d_r value in practice can be based on analyzing the diameter distributions of nanowires throughout a growth substrate. In this study, we constructed several groups of nano-FET devices, each group having a different d_r value. This makes sensitivity variations low within the group and much higher across groups.

The selection of $\Delta s_{\min}$ value influences success rates and also determines the number of qualified target nanowire candidates. A large $\Delta s_{\min}$ value results in higher nanomanipulation success rates but a smaller number of qualified target nanowire candidates, from which a nanowire with the desired d_r can be selected. Table 2 summarizes the average number of qualified target nanowire candidates with each nano-FET device at different $\Delta s_{\min}$ values, based on analyzing 500 nanowire devices before post-processing. It can be seen that the number of qualified target nanowire candidates within each device decreases significantly as the $\Delta s_{\min}$ value increases.

Table 3 summarizes the nanomanipulation failure rate for different $\Delta s_{\min}$ values. A higher $\Delta s_{\min}$ value means the target nanowire is well separated from other neighboring nanowires, resulting in a high success rate (e.g. 0% failure rate for $\Delta s_{\min} = 5$ and 3 μm). $\Delta s_{\min}$ was selected in our experiments to be 1 μm for a compromise between the nanomanipulation failure rate (4%) and the number of qualified target nanowire candidates (i.e. seven nanowires satisfying the $\Delta s_{\min}$ criterion and qualifying for final selection based on the desired nanowire diameter specification, d_r).

5.2. Varying number and diameter of nanowires

Automated nanomanipulation was used to post-process many nano-FET devices for controlling the number and

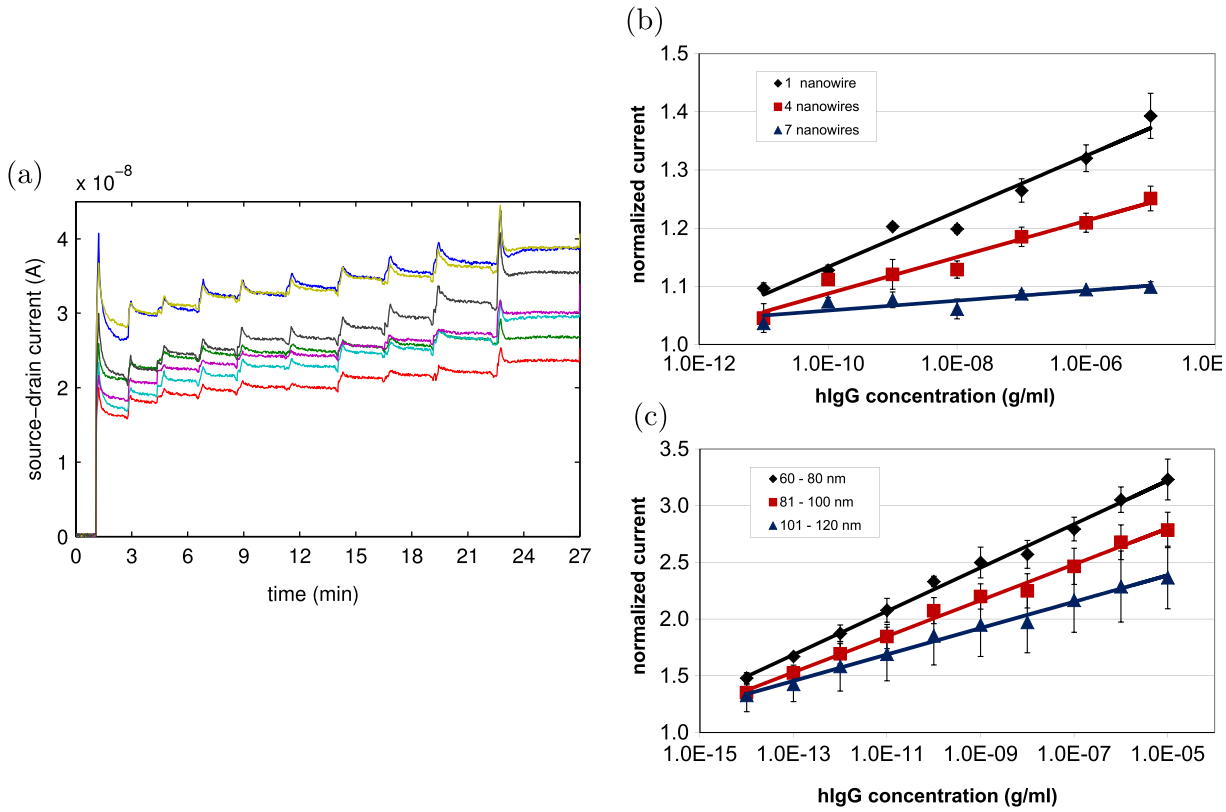

Figure 7. (a) A typical current–time response for seven Si-nanowire FET biosensors. Device current increased from a baseline value (dry device) upon subsequent addition of sample solution with increasing concentrations of hIgG in $0.1x$ PBS buffer (from 10 fg ml^{-1} to 10 μg ml^{-1}). (b) Effect of nanowire number on device sensitivity. Normalized current as a function of protein concentration for devices with one, four, and seven nanowires ($n = 4$ for each group; nanowire diameter = 81–100 nm). (c) Effect of nanowire diameter on device sensitivity. Single-nanowire devices with diameters ranging between 60 and 120 nm were characterized. Nanowire diameters were grouped into three categories: 60–80, 81–100, and 101–120 nm.

diameter of bridging nanowires. Nanowire devices were then functionalized with anti-human IgG for hIgG protein detection experiments. Nano-FET source–drain currents were measured as a function of increasing concentrations of hIgG protein ($V_{sd} = 0.01$ V, $V_{gate} = -1$ V). Figure 7(a) shows a few sets of raw measurement data. Figure 7(b) shows that the number of nanowires bridging source–drain electrodes incorporated into a nano-FET biosensor significantly affects device sensitivity (defined as $(I - I_0)/I_0$). Figure 7(c) shows quantitatively the nano-FET protein sensitivity dependence on nanowire diameters. It can be concluded that nano-FET devices having the same number of bridging nanowires and the bridging nanowires having similar diameters can have less sensitivity variation compared to devices with poorly controlled number and diameter of nanowires.

5.3. Success rate and efficiency

Figures 8(a) and (b) show a nano-FET device before and after robotic selective nanowire severing. Post-processing permits specific selection of desired nanowires and precise control of nanowire numbers. Figure 8(c) shows an array of nano-FET devices all having a single-nanowire bridging the source and drain electrodes. For a total of 500 trials, the

Table 4. Overall performance of nanorobotic manipulation.

Failure cases ($n = 500$)	Target NW broken	Networked
25	11	14
5%	44%	56%

success rate of the system was 95% (see table 4), as compared to 48.3% for manual nanomanipulation. Failure in robotic nanowire severing resulted from accidentally fracturing the target nanowire (2.2%) and the formation of an undesired nanowire network (i.e. removed 'nano-junk' landed on top of the target nanowire) (2.8%). Both nanowire networking and accidental target nanowire breakage were significantly lower compared to manual nanomanipulation as a direct result of precise execution of nanowire selection criteria and the high position performance of closed-loop position control.

The average time spent on post-processing a nano-FET device was ~1 min. Compared to the average speed of manual nanomanipulation (10.3 min/device), automated robotic nanowire manipulation improved the post-processing speed by ~10 times. Detailed break-up of the 1 min is: 9 s for nanowire detection and selection, 8 s for contact detection of the two nanoprobes, 22 s for position control of the two

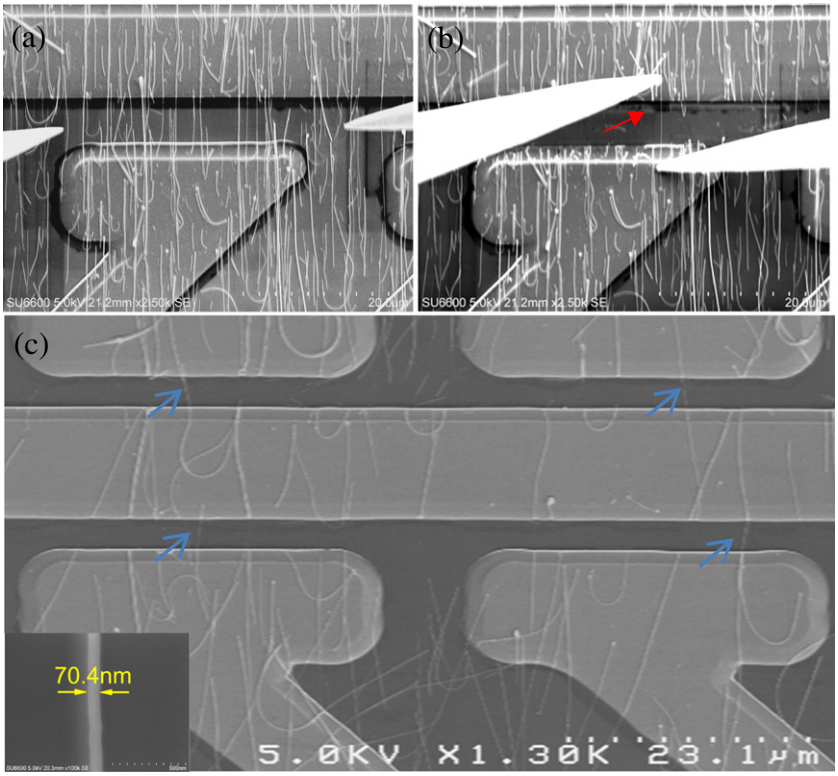

Figure 8. (a), (b) Before and after nanomanipulation removal of nanowires between source and drain electrodes. (c) An array of four single-nanowire devices (arrows: remaining nanowire). The inset shows a high-resolution SEM image of a target nanowire.

nanoprobes, and 20 s for probe cleaning. Typically, the tip of a nanoprobe requires cleaning after severing nanowires for three–four devices because of 'nano-junk'/contaminant build-up. Nanoprobe cleaning is at present manually conducted by touching the nanoprobe tip gently over a piece of carbon tape used an SEM sample fixation, which takes approximately 1 min. After processing about 20 devices, the nanoprobe tip was replaced because of significant contaminant build-up on the tip and/or because the probe tip became too thick for precision operation. Since replacing a nanoprobe can take minutes, we are presently pursuing approaches for *in situ* nanoprobe/tool exchange/replacement.

6. Conclusion

This paper presented a technique for batch microfabrication and serial post-processing of nanowire devices. The batch microfabrication process is wafer-scale but has an uncontrolled number of bridging nanowires that also have significantly varying diameters. Nanorobotic selective nanowire removal, despite being a serial process, permits precision control of the number and diameter of nanowires. Experimental results demonstrate that the nanorobotic system has a nano-FET device post-processing success rate of 95% (versus 48.3% for manual nanomanipulation) and has a speed of 1 min/device (versus 10.3 min/device). The significant improvement in both success rate and efficiency resulted from automated operation that enabled specific nanowire selection and precision position control.

Acknowledgments

This work was supported by the Natural Sciences and Engineering Research Council of Canada and by the Canada Research Chairs Program. The authors also thank Hitachi High-Technologies Canada Inc. for collaboration.

References

[1] Cui Y, Wei Q, Park H and Lieber C M 2001 Nanowire nanosensors for highly sensitive and selective detection of biological and chemical species *Science* **293** 1289–92
[2] Li Z, Chen Y, Li X, Kamins T I, Nauka K and Williams R S 2004 Sequence-specific label-free DNA sensors based on silicon nanowires *Nano Lett.* **4** 245–7
[3] Hahm J-I and Lieber C M 2004 Direct ultrasensitive electrical detection of DNA and DNA sequence variations using nanowire nanosensors *Nano Lett.* **4** 51–4
[4] Zhang G-J, Zhang L, Huang M J, Luo Z H H, Tay G K I, Lim E-J A, Kang T G and Chen Y 2010 Silicon nanowire biosensor for highly sensitive and rapid detection of dengue virus *Sensors Actuators* B **146** 138–44
[5] Zhang D, Liu Z, Li C, Tang T, Liu X, Han S, Lei B and Zhou C 2004 Detection of NO_2 down to ppb levels using individual and multiple In_2O_3 nanowire devices *Nano Lett.* **4** 1919–24
[6] Zhang Z, Hu C, Xiong Y, Yang R and Wang Z L 2007 Synthesis of Ba-doped CeO_2 nanowires and their application as humidity sensors *Nanotechnology* **18** 465504
[7] Gao Z, Agarwal A, Trigg A D, Singh N, Fang C, Tung C-H, Fan Y, Buddharaju K D and Kong J 2007 Silicon nanowire

arrays for label-free detection of DNA *Anal. Chem.* **79** 3291–7
[8] Elfstrom N, Karlstrom A E and Linnros J 2008 Silicon nanoribbons for electrical detection of biomolecules *Nano Lett.* **8** 945–9
[9] Stern E, Klemic J F, Routenberg D A, Wyrembak P N, Turner-Evans D B, Hamilton A D, LaVan D A, Fahmy T M and Reed M A 2007 Label-free immunodetection with CMOS-compatible semiconducting nanowires *Nature* **445** 519–22
[10] Li J, Zhang Y, To S, You L and Sun Y 2011 Effect of nanowire number, diameter, and doping density on nano-FET biosensor sensitivity *ACS Nano* **5** 6661–8
[11] Rao W S S G, Huang L and Hong S 2003 Nanotube electronics: large-scale assembly of carbon nanotubes *Nature* **425** 36–7
[12] Javey A, Nam S, Friedman R S, Yan H and Lieber C M 2007 Layer-by-layer assembly of nanowires for three-dimensional, multifunctional electronics *Nano Lett.* **7** 773–7
[13] Raychaudhuri S, Dayeh S A, Wang D and Yu E T 2009 Precise semiconductor nanowire placement through dielectrophoresis *Nano Lett.* **9** 2260–6
[14] Fukuda T, Arai F and Dong L 2003 Assembly of nanodevices with carbon nanotubes through nanorobotic manipulations *Proc. IEEE* **91** 1803–18
[15] Dong L, Arai F and Fukuda T 2004 Destructive constructions of nanostructures with carbon nanotubes through nanorobotic manipulation *IEEE/ASME Trans. Mechatronics* **9** 350–7
[16] Bell D J, Dong L, Nelson B J, Golling M, Zhang L and Grützmacher D 2006 Fabrication and characterization of three-dimensional InGaAs/GaAs nanosprings *Nano Lett.* **6** 725–9
[17] Mølhave K, Wich T, Kortschack A and Bøggild P 2006 Pick-and-place nanomanipulation using microfabricated grippers *Nanotechnology* **17** 2434–41
[18] Fukuda T, Nakajima M, Liu P and ElShimy H 2009 Nanofabrication, nanoinstrumentation and nanoassembly by nanorobotic manipulation *Int. J. Robot. Res.* **28** 537–47
[19] Dong L, Zhang L, Kratochvil B E, Shou K and Nelson B J 2009 Dual-chirality helical nanobelts: linear-to-rotary motion converters for three-dimensional microscopy *J. Microelectromech. Syst.* **18** 1047–53
[20] Cagliani A, Wierzbicki R, Occhipinti L, Petersen D H, Dyvelkov K N, Sukas Ö S, Herstrøm B G, Booth T and Bøggild P 2010 Manipulation and *in situ* transmission electron microscope characterization of sub-100 nm nanostructures using a microfabricated nanogripper *J. Micromech. Microeng.* **20** 035009
[21] Zhang Y, Liu X, Ru C, Zhang Y L, Dong L and Sun Y 2011 Piezoresistivity characterization of synthetic silicon nanowires using a MEMS device *J. Microelectromech. Syst.* **20** 959–67
[22] Chen B K, Zhang Y, Perovic D D and Sun Y 2011 MEMS microgripper with thin gripping tips *J. Micromech. Microeng.* **21** 105004
[23] Fatikow S, Wich T, Hülsen H, Sievers T and Jähnisch M 2007 Microrobot system for automatic nanohandling inside a scanning electron microscope *IEEE/ASME Trans. Mechatronics* **12** 244–52
[24] Ru C, Zhang Y, Sun Y, Zhong Y, Sun X, Hoyle D and Cotton I 2011 Automated four-point probe measurement of individual nanowires inside a scanning electron microscope *IEEE Trans. Nanotechnol.* **10** 674–81
[25] Zhang Y L, Zhang Y, Ru C, Chen B K and Sun Y, A load-lock-compatible nanomanipulation system for scanning electron microscope *IEEE/ASME Trans. Mechatronics* **35** 791–806
[26] Ji L and Yan H 2002 Attractable snakes based on the greedy algorithm for contour extraction *Pattern Recognit.* **35** 791–806